Chapter 3
Performance Enhancement of Rotors in Hover Using Fixed Gurney Flaps

Vasileios Pastrikakis, René Steijl, and George Barakos

Nomenclature

Latin

a Lift slope
c Blade mean chord [m]
u Mean velocity of the blade section relative to the fluid [m/sec]
c_p Pressure coefficient
c_T Thrust coefficient
c_Q Torque coefficient
c_t Sectional thrust coefficient
c_m Sectional moment coefficient
c_q Sectional torque coefficient
L_z Rotor loading along the span in the thrust direction [N/m]
L_m Rotor moment loading around the blade pitch axis [N]
L_q Rotor moment loading around the shaft axis [N]
M Mach number
N_b Number of blades
P_i Ideal induced rotor power [W]

V. Pastrikakis
Consulting Engineer, SoftInWay Switzerland GmbH
e-mail: v.pastrikakis@gmail.com

R. Steijl • G. Barakos (✉)
University of Glasgow, Glasgow, UK
e-mail: Rene.Steijl@glasgow.ac.uk; George.Barakos@glasgow.ac.uk

P	Actual rotor power [W]
R	Aspect ratio of the blade
FM	Figure of merit, FM $= P_i/P$

Greek

α	Angle of incidence [degrees]
β or β_0	Flapping angles [degrees]
γ	Rotor blade Lock number
θ or θ_0	Collective angle at 75%R [degrees]
λ	Inflow factor
μ	Advance ratio
ρ	Density [kg/m^3]
σ	Rotor solidity, $\sigma = N_b c/\pi R$

Acronyms

CFD	Computational fluid dynamics
MRB	Main rotor blade

3.1 Numerical Methods

3.1.1 Modelling Gurney Flaps

For the purposes of this study the Gurney flap on the W3-Sokol MRB is modelled by flagging any cell face within the computational mesh occupied by the flap with a solid, no-slip boundary condition. This method is implemented in the HMB3 solver and has been proved to be simple and effective.

In this case the Gurney is assumed to be thin, and is modelled along a block boundary. The same grid can be used for different size flaps as well as allowing unsteady deployment of Gurney flaps along block interfaces. The advantage of this method is that no additional effort is needed in terms of mesh generation.

3.1.2 Coupling with Structural Dynamics

For aeroelastic cases the blade was modelled as a beam and its static deformation was computed using Nastran 2005. The main structural properties needed for this analysis are the distributions of the sectional area, the chordwise and flapwise area

moments of inertia, the torsional stiffness, and the mass distribution along the span. The W3 MRB was modelled by 29 beam elements along the span and the properties were obtained by PZL Swidnik. At the root, the blade was free to flap but the lead-lag and pitching motion was not allowed. The twist of the blade was linear, $-10.6°/R$.

To account for fluid/structure coupling the aerodynamic loads are extracted from the fluid solution and used in NASTRAN as nodal forces to obtain the deformed blade shape. The blade along with the mesh is deformed based on the structural shape using a method described by Dehaeze and Barakos (2012). This method first deforms the blade surface using the constant tetrahedral volume (CVT) method. Then, it obtains the updated block vertex positions via spring analogy (SAM) and, finally, it generates the full mesh via a transfinite interpolation (TFI). The same process is repeated until the loads extracted from the flow solution are converged.

3.1.3 Trimming Method

A hover trimming method based on blade-element aeroelasticity was used for this study and was described by Steijl et al. (2006). The method requires the lock number γ_L of the blade and computes an initial trim state for a hovering rotor. After estimating the collective angle θ based on the thrust coefficient, the lift slope factor of the blade section, and the solidity of the rotor, the inflow factor λ is estimated, as well as the coning angle β. HMB2 is subsequently used to compute the thrust coefficient at this particular trimming before updating the collective and the coning based on the difference between the target and the estimated thrust coefficients. The procedure consists of the following steps:

1. At start-up two options can be used:

   (a) An initial estimate of the trim state is computed using the following equation for the collective pitch:

$$\theta_0 = \frac{6}{\sigma\alpha}C_T + \frac{3}{2}\sqrt{\frac{C_T}{2}}. \tag{3.1}$$

   (b) A user-defined initial guess for θ_0 is used.

   The inflow factor λ can be obtained directly from the equation:

$$\lambda = -\sqrt{\frac{C_T}{2}} = -\frac{\sigma\alpha}{16}\left[\sqrt{1 + \frac{64}{3\sigma\alpha}\theta_0} - 1\right]. \tag{3.2}$$

For a twisted rotor blade Eq. (3.2) gives the collective pitch at 0.75 of the rotor radius R. Then the equation for the coning angle is used:

$$\beta_0 = \frac{\gamma}{8}\left[\theta_0 + \frac{4}{3}\lambda\right].\tag{3.3}$$

2. The mesh is subsequently deformed to account for the new rotor blade incidence and position.
3. A steady flow simulation is performed until a prescribed level of convergence is reached.
4. The collective is updated using the following relation:

$$\delta\theta_0 = \frac{C_{T,\text{target}} - C_T}{dC_T/d\theta_0},\tag{3.4}$$

$$\frac{dC_T}{d\theta_0} = \frac{\sigma\alpha}{6}\left[1 - \frac{1}{\sqrt{1 + (64/3\sigma\alpha)\,\theta_0}}\right].\tag{3.5}$$

Equation (3.3) gives the coning angle for the new collective pitch $\theta_0 + \delta\theta_0$.

5. Steps 2–4 are repeated until a constant trim state is reached.

Therefore, the coning angle β_0 depends on the Lock number and the reduced model assumptions, while the collective is independent as only the derivation of the Newton iteration is dependent on the reduced aerodynamic model.

3.2 Hover Flight Calculations

3.2.1 W3-Sokol MRB Geometry

The W3-Sokol main rotor consists of four blades made out of fibre-glass. It is a soft blade in torsion that encourages the idea of the implementation of a gurney flap in order to alter the twist distribution along the radius of the blade. Figure 3.1 presents the geometry of the original MRB. The radius of the blade is along the x-axis and the leading-edge points towards the positive y-axis as the blade is rotating counter-clockwise. Although different sections of 5-digit NACA series are used along the radius, the basic section is the NACA23012M which is created by taking some camber out of the baseline NACA23012. At 0.678R of the blade there is a trim tab of 0.1c length and 0.07R span, while from 0.75R and up to the blade tip there is a trailing edge tab of 0.05c. The tip of the blade is rounded as shown in Fig. 3.1-III (upper panel). The MRB has a blunt trailing edge. All these geometrical characteristics increased the complexity of the generated mesh. Adding a fixed Gurney within the multiblock mesh topology would increase the number of nodes and would require additional computational cost to calculate even a steady hover case. For this reason the implementation of an infinitely thin Gurney flap was essential.
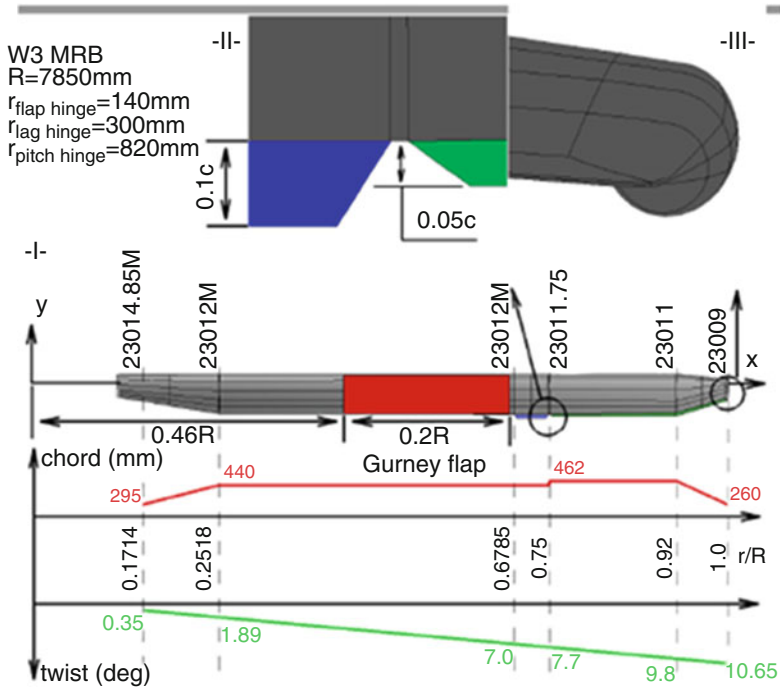
Fig. 3.1 (*I*) Geometry of W3-Sokol MRB, (*II*) close view at the trim tab and the trailing edge tab, (*III*) close view at the tip

For hover a Gurney flap of 0.01c was initially located at 0.46R. The span of the Gurney was 0.2R and its location and geometry are presented in Fig. 3.1-II (upper panel). The Gurney flap was flagged using the local mesh around the blade. This allows a normal to the trailing edge flap of infinite thickness to be simulated.

The mesh used for the hover calculations consists of 5.8 million nodes. A mesh convergence study suggested that this large number of cells was needed for the blade-loads to converge. It is a combined C-type topology in the y-plane with 402 nodes along the blade and O-type topology in the *x*-plane with 196 nodes around every section of the blade. In the normal direction of the blade 64 nodes have been used. The domain is split into 1360 blocks and it is presented in Fig. 3.2.

For the 4-bladed W3-Sokol rotor, the periodicity boundary condition in space and time is applied in a sector of $2\pi/4$ rad. At the farfield, the inflow, and the outflow surfaces the Froude condition for hover, presented by Wake and Baeder (1996) was applied. The farfield was located 52 chords away from the tip of the blade, while the inflow and outflow boundaries are located 30 and 60 chords away from the blade, respectively.
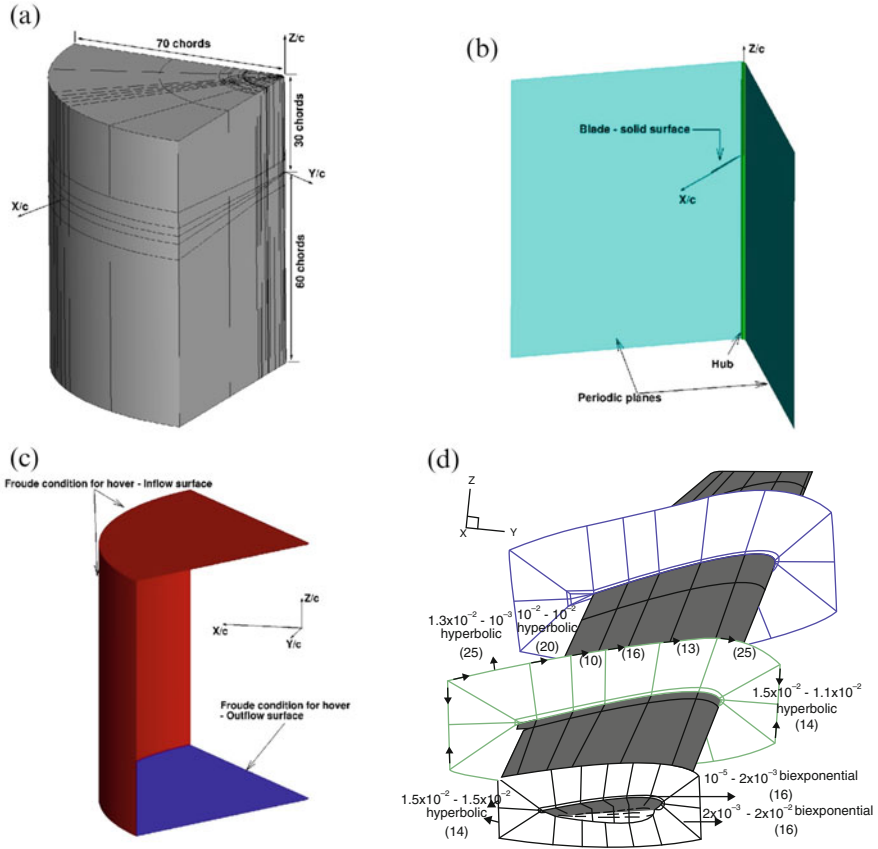
Fig. 3.2 CFD mesh and boundary conditions for the W3-Sokol rotor in hover. (**a**) Multiblock topology for a rotor in hover. (**b**) Detailed view of periodic planes. (**c**) Detailed view on inflow—outflow conditions. (**d**) Blocks around blade in hover. The numbers in brackets indicate number of nodes on the block edges

3.2.2 Rigid Blade Computations

3.2.2.1 Performance

Comparative performance calculations have been conducted at six different thrust targets for the rigid clean blade using the k-ω SST turbulence model. The collective and coning angles used at every case are presented in Table 3.1. The maximum FM was 0.74 and it was observed at medium thrust settings ($C_T/\sigma = 0.185$). At the same setting the torque coefficient was $C_Q = 0.001$.

The hover performance for the clean blade as well as the blade with Gurney flaps can be seen in Figs. 3.3 and 3.4, and an enlarged view is presented in Fig. 3.5. Three vertical lines are also drawn in that figure corresponding to estimated weight

Table 3.1 Control angles
and target thrust coefficients
for the clean W3-Sokol blade
and the blade with fixed
Gurney flap of 2% of the
chord (in brackets) in hover

Case	θ_0 [deg]	β_0 [deg]	C_T
1	4.5 (3.6)	1.5 (0.6)	0.0045
2	7.0 (6.1)	2.5 (1.8)	0.0082
3	10.0 (9.1)	5.0 (4.1)	0.0132
4	11.5 (10.5)	6.0 (5.2)	0.0154
5	14.0 (12.9)	6.2 (5.5)	0.0189
6	16.0 (14.4)	10.0 (8.7)	0.0209

Fig. 3.3 Figure of merit
versus thrust coefficient for
the W3-Sokol MRB in hover
($M_{tip} = 0.618$,
$Re_{tip} = 3.74 \times 10^6$,
$\sigma = 0.0714$)
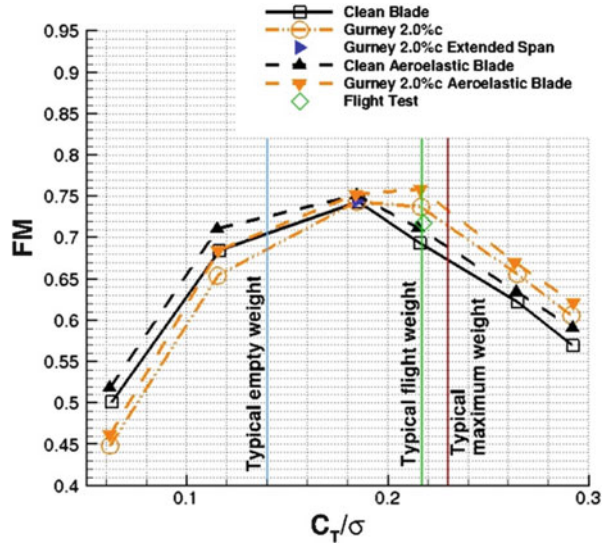
cases for a typical helicopter like the W3-Sokol. In fact, the green line represents
hover data provided by PZL Swidnik in order to validate the CFD methods. As
demonstrated in Fig. 3.6a about 200,000 iterations were needed for a well-converged
solution. If the trimmer was also employed, it added an additional number of
iterations since after every re-trim the flow needs to adjust and further steps to
converge.

3.2.2.2 Analysis of Rigid Blade Results

In Fig. 3.7a the surface pressure coefficient is presented and in Fig. 3.7b the C_P plots
at three different sections for the clean blade can be seen. The $r/R = 0.56$ station is
where the Gurney flap will be located, while in the $r/R = 0.73$ section the expected
effect of the blade trim tab is observed. The trailing edge tab seems to have a similar
effect, which can be seen from the pressure distribution at $r/R = 0.89$.

In Fig. 3.8a the wake of the blade is visualised using the vorticity magnitude of
0.1 s^{-1}, which shows that the vortex created at the tip of the blade interacts with
the following blade at near 0.89R, due to the wake contraction. After calculating the

Fig. 3.4 Torque versus thrust coefficient for the W3-Sokol MRB in hover ($M_{tip} = 0.618$, $Re_{tip} = 3.74 \times 10^6$, $\sigma = 0.0714$)
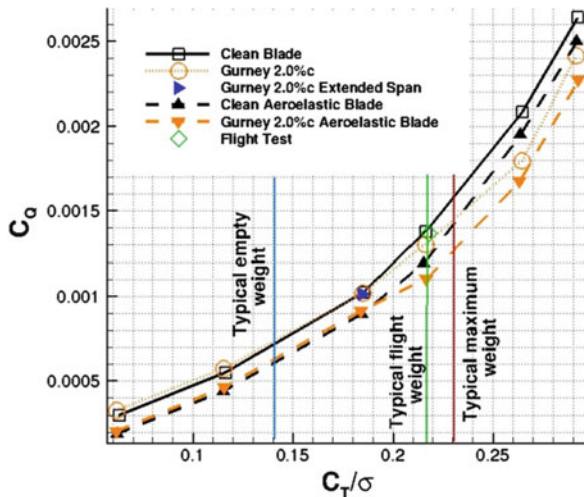
Fig. 3.5 Estimated benefit in hover flight when a Gurney flap is deployed ($M_{tip} = 0.618$, $Re_{tip} = 3.74 \times 10^6$, $\sigma = 0.0714$)
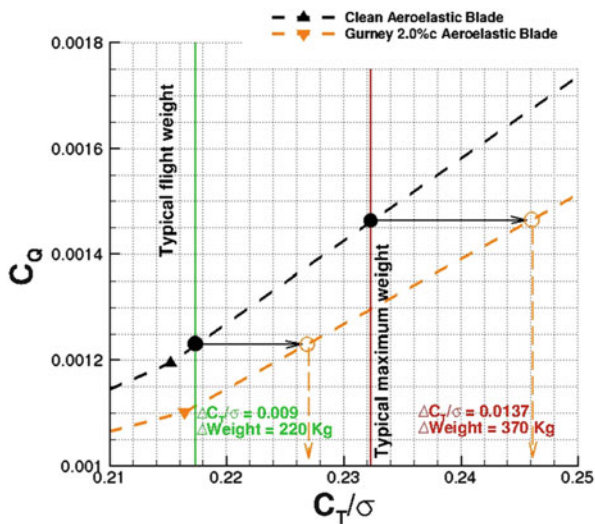
performance of the W3 rotor in hover, a Gurney flap of 0.2R span was implemented at $r/R = 0.46$ of the blade. The height of the flap varied from 0.3%c up to 2%c and the flap was assumed to be infinitely thin. Hover calculations were conducted for six thrust settings and the HMB3 trimmer was used to force the blade to reach the same thrust as the clean blade. It is pointed out that the Gurney improves the performance of the rotor above medium thrust ($C_T/\sigma = 0.185$). The most beneficial Gurney size is 2% of the chord and the maximum benefit in figure of merit was $+0.044$ at $C_T = 0.0154$ ($C_T/\sigma = 0.216$) which corresponds to 6.3% increase compared to the clean case. These results can be seen in Fig. 3.3. The Gurney effect on the wake of the blade is well captured and it is presented in Fig. 3.8b using the isosurface of

(a)

(b)
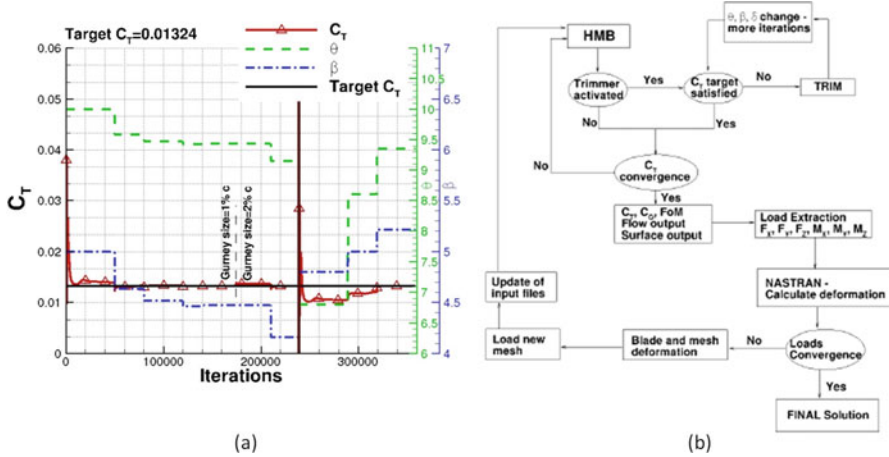
Fig. 3.6 (**a**) Convergence history for thrust coefficient, collective, and coning angle during aeroelastic hover computations along with trimming process. (**b**) Flow chart for aeroelastic calculations in hover

(a)

(b)
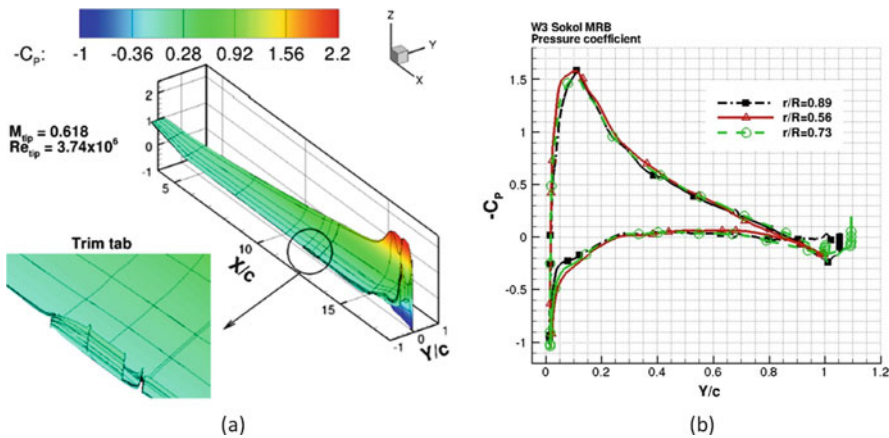
Fig. 3.7 (**a**) Pressure coefficient along the W3 MRB and (**b**) pressure coefficient at different sections of the blade normalised using the local dynamic head, $\theta = 10°$, $\beta = 5°$, $C_T = 0.0132$, FM $= 0.7432$, $C_Q = 0.001$

vorticity magnitude equal to $0.1\ \text{s}^{-1}$. For the clean case only the vortices created by the trim tab and the tip of the blade are obvious, while on the blade with the fixed Gurney the vortex generated due to the flap is observed inboard.

In Fig. 3.9a, b the pressure coefficient on the blade surface is presented for the blade with and without a Gurney flap. The effect of the flap on the decrease of the pressure on the suction side and the increase of the pressure on the pressure side is clear, although this effect decays rapidly away from the tips of the flap. A further comparison is conducted between the sectional pressure coefficients of both blades

Fig. 3.8 Wake visualisation
on W3 MRB (**a**) without and
(**b**) with Gurney flap in hover
by using the isosurface of
vorticity magnitude equal to
0.1 s^{-1}, $\theta_0 = 10°$, $\beta = 5°$,
$C_T = 0.0132$, FM $= 0.7432$,
$C_Q = 0.001$
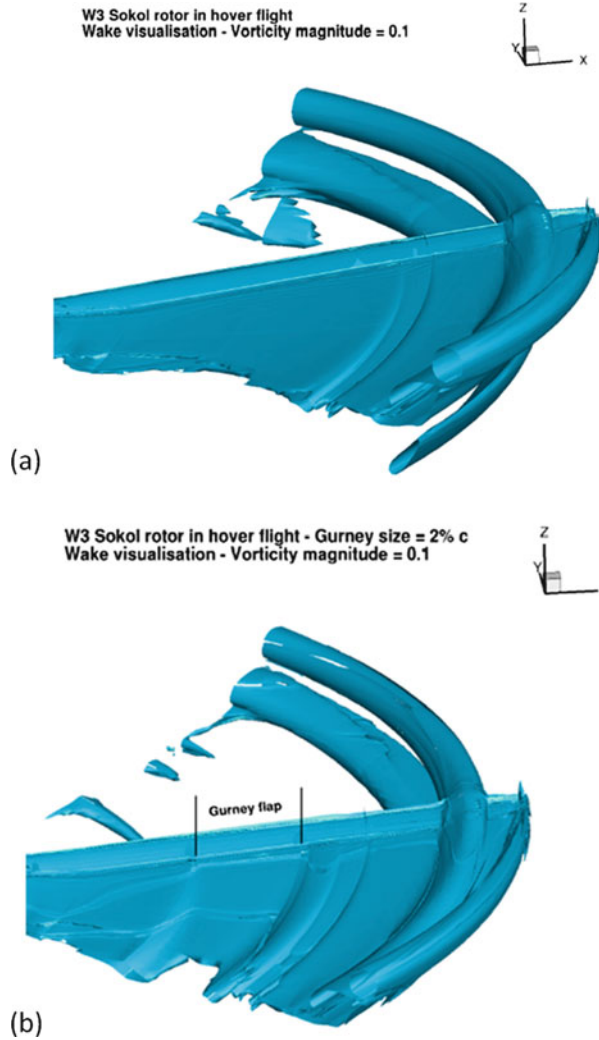
in Fig. 3.10. It shows that a Gurney of 2% of the chord alters the pressure distribution
at almost 80% of the sectional surface. At lower thrust where the collective of the
blade is not very high the Gurney extends more out of the boundary layer and creates
additional drag leading to a decrease of the blade performance.

Fig. 3.9 Pressure distribution on upper and lower surface of W3 MRB without Gurney (**a**) and with Gurney (**b**). Clean blade: $\theta = 11.5°$, $\beta = 6°$, $C_T/\sigma = 0.216$, FM $= 0.6934$, $C_Q = 0.00138$. Blade with Gurney flap: $\theta = 10.46°$, $\beta = 5.21°$, $C_T/\sigma = 0.216$, FM $= 0.7374$, $C_Q = 0.00129$
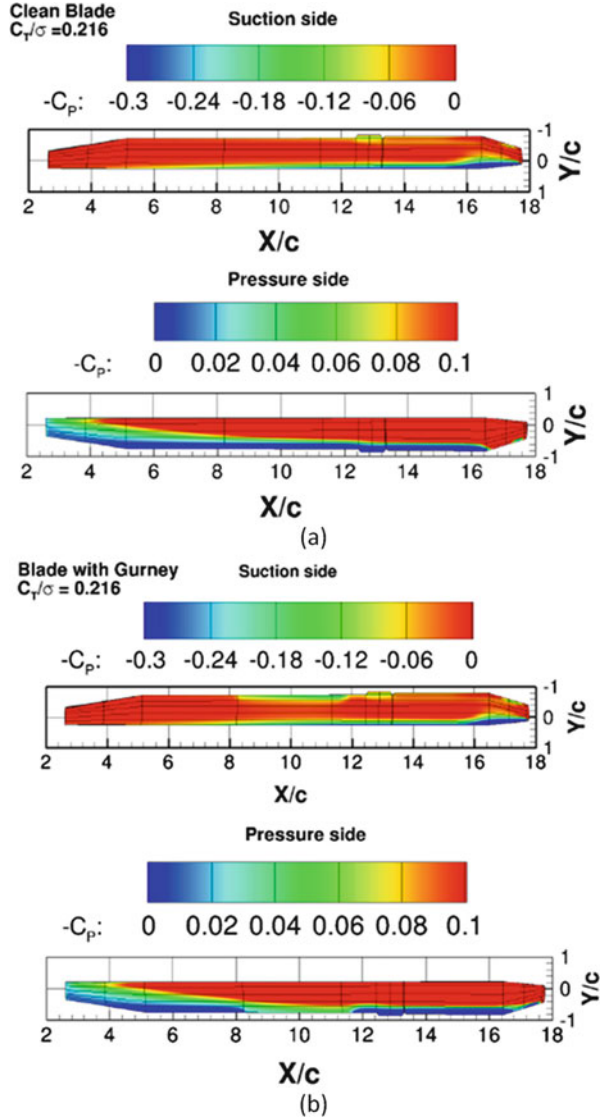
3.2.3 Aeroelastic Calculations

3.2.3.1 Application of the Aeroelastic Method and Trimming

Given the sectional properties of the blade, aeroelastic calculations were conducted at the same thrust settings. In Fig. 3.11 the blade is modelled using beam elements in NASTRAN to calculate the deformed shape according to the loads extracted from the flow solution. The structural properties of the blade are presented in Fig. 3.12

Fig. 3.10 Pressure
coefficient at
$r/R = 0.56$—comparison
between clean blade and
blade with Gurney flap
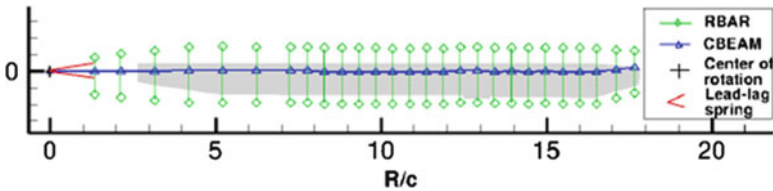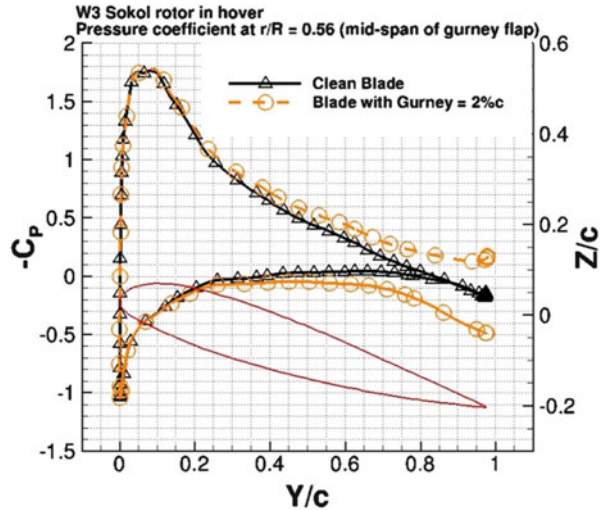
Fig. 3.11 Structural model of the W3-Sokol blade used in NASTRAN

which suggests that this blade is soft compared to more modern designs. Especially, the beamwise and the torsional stiffness are very low compared to the chordwise stiffness along the radius which allows the blade to flap and to twist more during flight.

The process of getting the final converged solution is summarised in Fig.3.6b. Having obtained the converged solution for the rigid blade the aerodynamic loads along the blade are extracted and NASTRAN is used to obtain the new deformed shape using a non-linear analysis. The mesh is then deformed according to that shape and the flow-field is updated until convergence. The trimmer is then employed to reach the required thrust coefficient and the same process is repeated until the loads converge.

3.2.3.2 Analysis of Elastic Blade Results

The black dots in Fig. 3.3 correspond to the aeroelastic calculations performed for the W3 MRB and the performance of the blade is improved. The agreement between the estimated FM and this of tests is also better. The reason for the aerodynamic enhancement is partly due to the structural properties of the blade which allow some

Fig. 3.12 Structural properties of the W3-Sokol blade used in NASTRAN
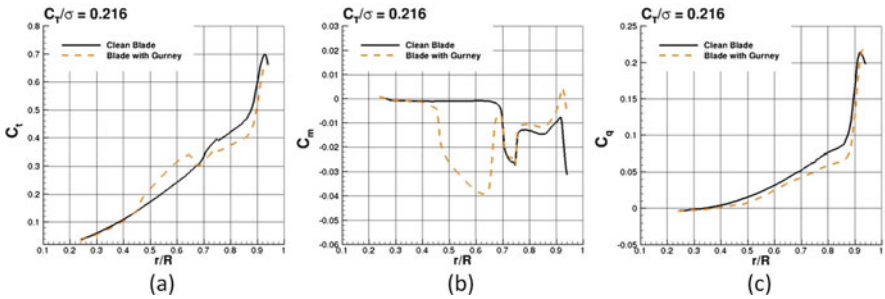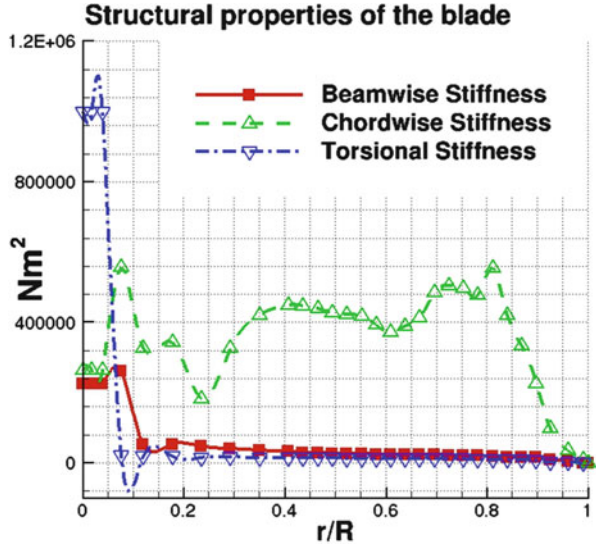
Fig. 3.13 (**a**) Sectional thrust coefficient, (**b**) pitching moment coefficient, and (**c**) torque coefficient of the W3 MRB with (*dashed line*) and without Gurney flap (*solid line*). Clean blade: $\theta = 11.5°$, $\beta = 6°$, $C_T/\sigma = 0.216$, FM = 0.6934, $C_Q = 0.00138$. Blade with Gurney flap: $\theta = 10.46°$, $\beta = 5.21°$, $C_T/\sigma = 0.216$, FM = 0.7374, $C_Q = 0.00129$

twist, and as a consequence, the higher twist leads to a higher figure of merit in hover as mentioned in studies by Keys et al. (2000) and Gagliardi and Barakos (2009). In Fig. 3.13 the effect of the Gurney flap on the sectional thrust, pitching moment, and torque coefficients is presented at the point where the maximum positive effect was captured. These curves were drawn using the aerodynamic loads extracted at 100 different sections along the MRB. The filled squares and the open circles correspond to the loads applied on the nodes used in the structural model. The Gurney increased the sectional thrust locally near its location, but the integrated average thrust remained the same due to trimming. As far as the torque is concerned, the Gurney flap decreased the requirements more.

At the same time the Gurney flap introduced more nose-down moments which tend to lower the collective by more than 1° as presented in Fig. 3.14. Although the

σ=0.0714
Rigid W3 Sokol rotor in hover flight
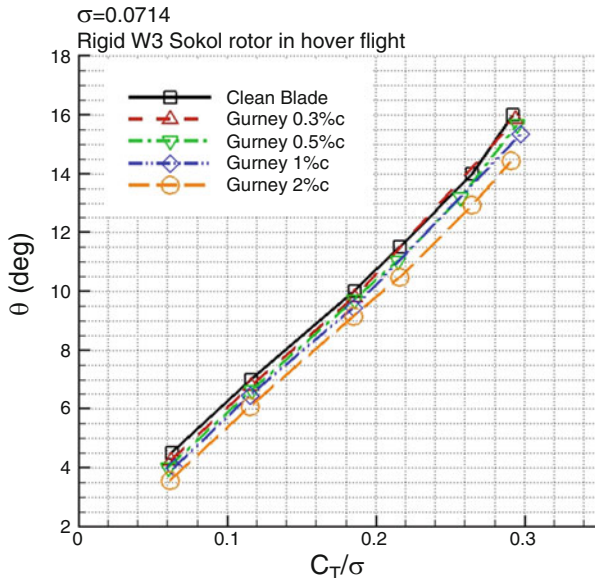
Fig. 3.14 Collective angle after trimming versus C_T/σ for different Gurney sizes on the W3 MRB in hover

Fig. 3.15 Lift over drag comparison for a NACA23012 aerofoil with (*dashed line*) and without a Gurney flap (*solid line*)

NACA23012
Re = 3x10^6
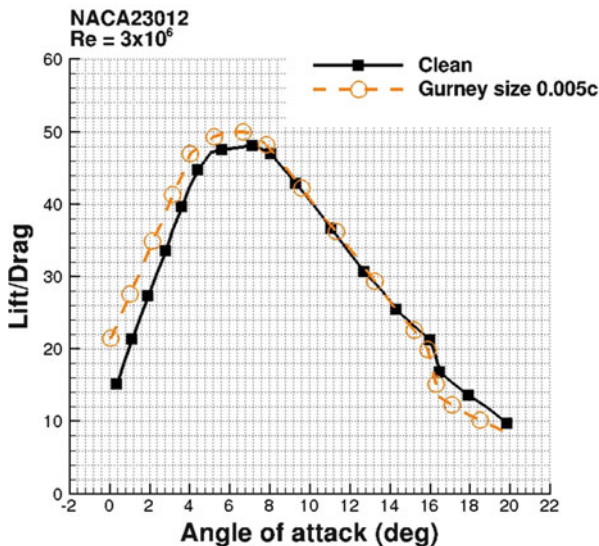
collective of the blade was further decreased by using a Gurney the overall thrust capability of the blade was maintained as extra lift was provided by the flap. This can also be explained in Fig. 3.15, which compares the lift over drag ratio for a clean NACA23102 and Gurneyed one at different incidence.

Fig. 3.16 Change of twist distribution for W3 MRB with and without Gurney flap in hover
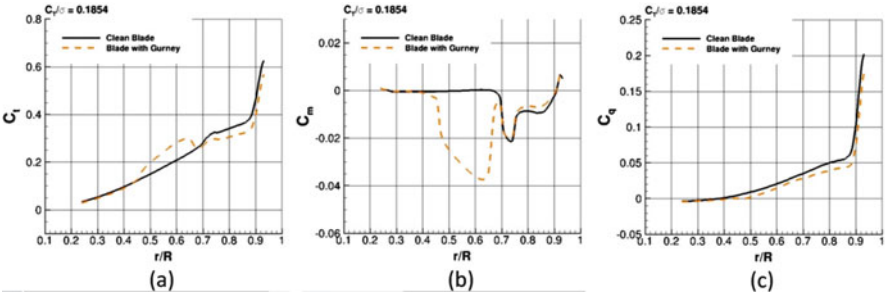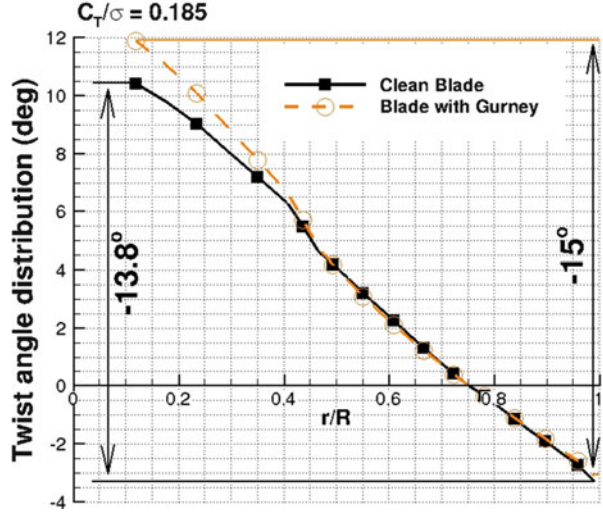
Fig. 3.17 (**a**) Sectional thrust coefficient, (**b**) pitching moment coefficient, and (**c**) torque coefficient of the W3 MRB with (*dashed line*) and without Gurney flap (*solid line*). Clean blade: $\theta = 10.0°$, $\beta = 5°$, $C_T/\sigma = 0.1853$, FM $= 0.7432$, $C_Q = 0.001$. Blade with Gurney flap: $\theta = 9.15°$, $\beta = 4.16°$, $C_T/\sigma = 0.1853$, FM $= 0.7429$, $C_Q = 0.001$

Finally, in Fig. 3.16, the change of the twist for both the clean blade and the blade with a Gurney flap is presented to justify the positive aerodynamic effect of the gurney by further increasing the twist by 1.2°. These results correspond to the hover case where the Gurney flap had the most beneficial effect ($C_T/\sigma = 0.216$).

The corresponding results to the lower and higher thrust cases are presented in Figs. 3.17 and 3.18. The effect of the Gurney is quantified in Fig. 3.5. For a given torque requirement it is obvious that using the Gurney a higher thrust coefficient can be reached. This C_T increase for the case of flight test data corresponds to a weight increase of 220 kg.
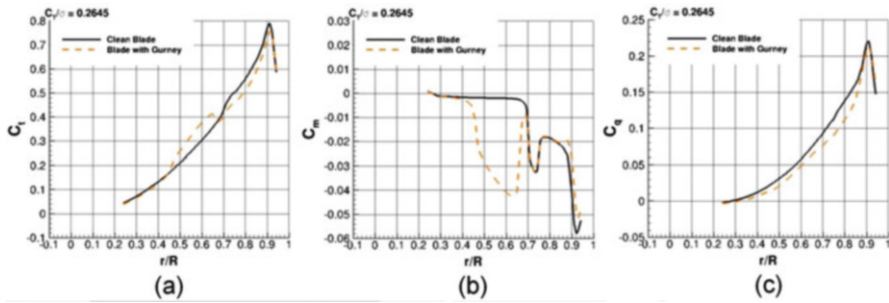
Fig. 3.18 (**a**) Sectional thrust coefficient, (**b**) pitching moment coefficient, and (**c**) torque coefficient of the W3 MRB with (*dashed line*) and without Gurney flap (*solid line*). Clean blade: $\theta = 14°$, $\beta = 6.2°$, $C_T/\sigma = 0.264$, FM = 0.622, $C_Q = 0.0021$. Blade with Gurney flap: $\theta = 12.92°$, $\beta = 7.36°$, $C_T/\sigma = 0.264$, FM = 0.656, $C_Q = 0.0017$

3.3 Conclusions

In this chapter the use of a Gurney flap was put forward as a means to improve the hover performance of a helicopter rotor. The basic idea is that the flap will be retracted in forward flight and deployed in hover flight only. The W3-Sokol MRB was used in this work due to the availability of the blade shape and structural properties. The maximum FM of the blade did not improve, but at high thrust settings it was enhanced by 6% over the performance of the clean blade. The effect of the Gurney flap to pitch the nose of the section down was evaluated with aeroelastic calculations and it was found that the extra lift of the Gurney in combination with the extra blade twist resulted in an increased FM. For further performance improvement a Gurney flap of bigger span could be considered. Among different sizes of Gurney the one of 2% of the chord was the most effective.

In the future, computations using a fuselage are considered and the location of the Gurney will be further optimised to maximise blade performance. The interaction of the wake generated by the rotor blade with the fuselage may affect the rotorcraft performance in such a way that relocation or a change of the Gurney size may be essential. In addition, the effect of adding a mechanism for the flap actuation on the blade structural properties should be investigated.

References

Dehaeze F, Barakos GN (2012) Hovering rotor computations using an aeroelastic blade model. Aeronaut J 49(1):82–92

Gagliardi A, Barakos GN (2009) Analysis and design of a flap-equiped low-twist rotor in hover. J Aircr 46(1):74–84

Keys C, Tarzanin F, McHugh DW (2000) Effect of twist on helicopter performance and vibratory loads. In: 13th European Rotorcraft Forum. Arles, France

Nastran MSC (2005) Quick Reference Guide. MSC Software Corporation

Steijl R, Barakos GN, Badcock K (2006) A framework for CFD analysis of helicopter rotors in hover and forward flight. Int J Numer Methods Fluids 51(8):819–847

Wake BE, Baeder JD (1996) Evaluation of a Navier-Stokes analysis method for hover performance prediction. J Am Helicopter Soc 41:7–17